A novel extension of Frantz–Nodvik laser-amplifier model: a computational study

Alireza Heidari, Fatemeh Ghorbani, and Mohammadali Ghorbani*

Institute for Advanced Studies, Tehran 14456-63543, Iran

Abstract. The Frantz–Nodvik model was extended to propagate pulse through a double-pass laser amplifier and to study beam-interaction effects on the output-energy fluence and gain factor according to the distance between two beams. We also obtained the necessary approximation equations for the saturation state and small input pulse. The results show that minimum output energy and gain occur when two beams completely coincide. The comparison between numerical, analytical, and empirical results demonstrates a good correspondence.

1   Introduction

Increasing efficiency and decreasing amplifier levels are of great significance particularly in laser-joint systems, and an appropriate analytical model can successfully be used to optimize the design of such optical structures. In practice, double- or multi-pass amplifiers functionally amplify extremely low- and high-energy pulses [1–3]. Most analytical models that have been proposed for optical amplifiers are based on the Frantz–Nodvik theory [4]. In this model, only by assuming that the gain factor depends on the direction of laser beam propagation through the amplifying medium, the relationship between input- and output-energy fluxes is obtained according to the initial gain factor and saturation-energy flux. Modifying the gain factor, this model is used again for the second pass [5]. By providing a simple analysis and assuming that the initial distribution of gain is uniform throughout the active medium, the Frantz–Nodvik model leads to very good results for explaining the amplifier's behavior. When the laser pulse width (t_p)

---

*Corresponding author. *Email address:* mohammadalighorbani1983@yahoo.com (M. Ghorbani)

is much larger than the time necessary for the optical pulse to pass through the amplifier (τ) and the gain slightly changes during pulse pass due to pumping and under-drop mechanisms, the Frantz–Nodvik model that is independent of input pulse's temporal behavior and the laser active medium's type is valid and employed [6–9]. When the gain distribution is not uniform due to the amplifier's non-uniform pumping or the radial dependence of the distribution of input intensity, a special accuracy is required to employ the Frantz–Nodvik model [10–13]. In such instance, by assuming that the gain spatial distribution is known before the optical pulse enters the amplifier, the one pass version of this model can be used for every point inside the amplifier. The transverse distribution of output-beam intensity can be obtained by iterating this model. For consecutive passes and the assumption that $t_p \gg \tau$, the optical gain of each beam is affected by its neighboring beams' intensity. In this case, except for a special state in which the beams' propagation directions coincide [14], there is not any appropriate analytical model to describe how the output-energy flux depends on the distance between beams' propagation directions [15–20]. The only existing model of multi-pass amplifiers provides necessary calculations just by qualitative and approximate considerations concerning beams overlapping and regardless of passing beams' spatial position [21]. Hence, for appropriate initial and boundary conditions on the amplifier's input and output surfaces, the mass contrast and photon flux of each beam can be obtained only through numerically solving the position-dependent rate equations [22–25].

In this paper, for the first time, after solving the rate equations for a double-pass amplifier, we obtain the analytical solutions for the dependence of input-energy fluence on the radial-position-dependent optical gain and transmission factor between the first pass and second pass, and the fluence of output energy to gain for the known directions of input and output beams. The obtained results are consistent with the numerical and empirical results.

2   Position-dependent rate equations for double-pass amplifiers

When the input beam's temporal width is small enough compared with the upper level's lifetime and active medium's pumping time, the following simplified rate equations can be used to obtain the mass contrast between the active medium's upper and down levels ($N(r,z,t)$) and the photon density of first and second passes ($\Phi_1(r,z,t)$ and $\Phi_2(r,z,t)$) [10]

$$\frac{\partial}{\partial t}\Phi_1(r,z,t) + c\frac{\partial}{\partial z}\Phi_1(r,z,t) = N(r,z,t)\,c\sigma\Phi_1(r,z,t) \tag{1}$$

$$\frac{\partial}{\partial t}\Phi_2(r,z,t) - c\frac{\partial}{\partial z}\Phi_2(r,z,t) = N(r,z,t)\,c\sigma\Phi_2(r,z,t) \tag{2}$$

$$\frac{\partial}{\partial t}N(r,z,t) = -N(r,z,t)\,c\sigma\left[\Phi_1(r,z,t) + \Phi_2(r,z,t)\right] \tag{3}$$

In addition to radial position (r), the mass contrast and photon density are a function of spatial position along the beam propagation direction (z) and time (t). Eqs. (1) and (2) show the transport of photons along z in which Φ_1 and Φ_2 respectively propagate along the positive and negative directions of z and in the distance r_1 and r_2 from z. The parameter c denotes the propagation speed of the laser field into the active medium and σ represents the induced-emission cross section.

3 Solving rate equations

By removing the nonlinear terms in Eqs. (1)–(3), and integrating them over the amplifier length from $z=0$ to $z=L$, we obtain

$$\Phi_2(r,L,t)-\Phi_2(r,0,t)-\Phi_1(r,L,t)+\Phi_1(r,0,t)=\frac{1}{c\sigma}\int_0^L \frac{\partial}{\partial t}N(r,z,t)\sigma dz \qquad (4)$$

First, we divide both sides of (4) by the input-photon density at $r=r_1$, or $\Phi_1(r_1,0,t)$

$$\frac{\Phi_2(r,L,t)}{\Phi_1(r_1,0,t)}-\frac{\Phi_2(r,0,t)}{\Phi_1(r_1,0,t)}-\frac{\Phi_1(r,L,t)}{\Phi_1(r_1,0,t)}+\frac{\Phi_1(r,0,t)}{\Phi_1(r_1,0,t)}=\frac{1}{c\sigma\Phi_1(r_1,0,t)}\int_0^L \frac{\partial}{\partial t}N(r,z,t)\sigma dz \quad (5)$$

According to (6) and (7), the small-signal gain, $G(r,t)$, is dependent on the photon density and mass contrast between the active medium's energy levels

$$G(r,t)=\frac{\Phi_1(r,L,t)}{\Phi_1(r,0,t)}=\frac{\Phi_2(r,0,t)}{\Phi_2(r,L,t)} \qquad (6)$$

$$G(r,t)=e^{\int_0^L N(r,z,t)\sigma dz} \qquad (7)$$

The beam-transfer function (ψ), which connects the first-pass output beam to the second-pass input beam by assuming that the laser pulse's temporal behavior does not or slightly changes from the first exit to second entry (this assumption is often appropriate), is a function of the transmission of parts after the amplifier (T) and beams' radial position

$$\psi(r,T)=\frac{\Phi_2(r,L,t)}{\Phi_1(r,L,t)} \qquad (8)$$

The radial dependence of the photon density in the first and second passes are shown by $f_1(r,z)$ and $f_2(r,z)$, respectively

$$\Phi_1(r,z,t)=f_1(r,z)\Phi_1(r_1,z,t) \qquad (9)$$

$$\Phi_2(r,z,t)=f_2(r,z)\Phi_2(r_2,z,t) \qquad (10)$$

By inserting (6), (8), and (9) into (5), we get

$$G(r_1,t)\psi(r,T)-\psi(r,T)G(r_1,t)G(r,t)-G(r,t)+1=\frac{1}{c\sigma\Phi_1(r,0,t)}\frac{\partial}{\partial t}\int_0^L N(r,z,t)\sigma dz \quad (11)$$

The saturation-energy fluence, J_S, is defined as

$$J_S=\frac{\hbar\omega}{\sigma} \quad (12)$$

where $\hbar\omega$ represents the laser-transition photon energy. By inputting (12) to (11), the equation required to connect the input-photon density, gain factor, and beam-transfer function is obtained

$$c\hbar\omega\Phi_1(r,0,t)=\frac{J_s\frac{\partial}{\partial t}\int_0^L N(r,z,t)\sigma dz}{[1+G(r_1,t)\psi(r,t)]+[1-G(r,t)]} \quad (13)$$

Now, both sides of (4) is divided by $\Phi_2(r_2,0,t)$. Similarly to the calculations led to (13), and using $G(r,t)$, $\psi(r,T)$, and (10), we get the equation below for the output-photon density

$$c\hbar\omega\Phi_2(r,0,t)=\left(\frac{J_sG(r_2,t)\psi(r,T)}{\psi(r,T)[1-G(r_2,t)]-1}\right)\frac{\frac{\partial}{\partial t}\int_0^L N(r,z,t)\sigma dz}{1+\left[\frac{1}{\psi(r,T)[1-G(r_2,t)]-1}\right]\frac{1}{G(r,t)}} \quad (14)$$

The fluence of input and output energies can be achieved by integrating the photon density at $z=0$

$$J_{in}(r)=\int_{-\infty}^{\infty}\hbar\omega c\Phi_1(r,0,t)dt \quad (15)$$

$$J_{out}(r)=\int_{-\infty}^{\infty}\hbar\omega c\Phi_2(r,0,t)dt \quad (16)$$

When the period of time each beam passes the active medium is much shorter than the laser pulse width, which is usually for laser pulses with temporal width of the order of 10^{-8}s or more, we can neglect the temporal dependence of G and consider the gain to be only a function of position as $G(r)$. This assumption will be applied to all the calculations of the sections 3.1, 3.2, and 4.

3.1 Propagating beams along one direction for two passes

In the special state, beams' directions coincide ($r=r_1=r_2$); consequently, $G(r)=G_1(r,r_1)=G_2(r,r_2)$. Because (1), (2), and (3) do not contain derivative with respect to r and considering $u(r,t)=\int_0^L N(r,z,t)\sigma dz$, we can use the equation below for each r. The effect of radial position r on the gain is inserted into the calculations by the function ψ

$$du = \left[\frac{\partial}{\partial t} \int_0^L N(r,z,t) \sigma dz \right] dt \tag{17}$$

The integration of (13) and (14) is possible using (7), (15), and (16). The following equations give the relationship between J_{in} and J_{out} for every known value of r through the parameter G

$$\exp\left(\frac{J_{in}(r)}{J_s} \right) = \left[\frac{G(r)}{G_0} \right] \left[\frac{G(r)-1}{G_0-1} \right]^{-\frac{1}{1+\psi}} \left[\frac{G(r)\psi+1}{G_0\psi+1} \right]^{-\frac{\psi}{(1+\psi)}} \tag{18}$$

$$\exp\left(\frac{J_{out}(r)}{J_s} \right) = \left[\frac{G(r)-1}{G_0-1} \right]^{-\frac{\psi^2}{1+\psi}} \left[\frac{G(r)\psi+1}{G_0\psi+1} \right]^{-\frac{\psi}{(1+\psi)}} \tag{19}$$

where G_0 is the initial gain of small signal in the active medium, which is constant and dependent of position. By dividing (19) by (18), we get the relationship between the input fluence and output fluence

$$J_{out}(r) = J_{in}(r) + J_s \left[\ln\left(\frac{G_0}{G(r)} \right) + (\psi-1)\ln\left(\frac{G_0-1}{G(r)-1} \right) \right] \tag{20}$$

By combining (18) and (19), we can make them similar to the Frantz–Nodvik classical equation as far as possible

$$\frac{e^{(1+\psi)\left(\frac{J_{out}(r)}{J_s} \right)} - 1}{e^{(1+\psi)\left(\frac{J_{in}(r)}{J_s} \right)} - 1} = \frac{\left(\frac{G_0-1}{G(r)-1} \right)^{\psi^2} \left(\frac{\psi G_0+1}{\psi G(r)+1} \right)^{\psi} - 1}{\left(\frac{G(r)}{G_0} \right)^{\psi+1} \left(\frac{G_0-1}{G(r)-1} \right) \left(\frac{\psi G_0+1}{\psi G(r)+1} \right)^{\psi} - 1} \tag{21}$$

For the special case $\psi = 1$ and the uniform distribution of input-photon fluence, in which all the output beam returns to the amplifier for the second pass without any change, (21) is reduced to (22) for the double-pass amplifier at the limit state $r_1 = r_2$ for $T = 1$ [10]

$$\frac{e^{\left(\frac{2J_{out}}{J_s} \right)} - 1}{e^{\left(\frac{2J_{in}}{J_s} \right)} - 1} = G_0^2 \tag{22}$$

There is another special case at $\psi = 0$ in which the first-pass output beam does not return to the amplifier anymore. In other words, the transmission is zero between the two passes, $T = 0$. In this state, (21) gives $J_{out} = 0$, which is correct.

3.2　Propagating beams along two different directions

When two beams' directions do not coincide, the Frantz–Nodvik theory leads to an appropriate approximation for the gain during each pass ($r = r_1$, $r = r_2$), which can be used for G_1 and G_2 in order to integrate (13) and (14) [4]

$$G_1 = \frac{G_0 e^{\frac{J_{in}(r_1)}{J_s}}}{(1-G_0) + G_0 e^{\frac{J_{in}(r_1)}{J_s}}} \tag{23}$$

$$G_2 = \frac{G_0 e^{\frac{J_{in2}(r_2)}{J_s}}}{(1-G_0) + G_0 e^{\frac{J_{in2}(r_2)}{J_s}}} \tag{24}$$

where $J_{in2}(r_2)$ denotes the fluence of the second-pass input energy

$$J_{in2}(r_2) = TJ_{in}(r_1)G_1 \tag{25}$$

Therefore, (13) and (14) bring about (26) and (27)

$$J_{in}(r) = \frac{J_S}{[1 + G_1 \psi(r)]} \int_{\ln G_0}^{\ln G} \frac{du}{1 - e^u} \tag{26}$$

$$J_{out}(r) = J_s \left(\frac{\psi(r) G_2}{\psi(r)[1-G_2]-1} \right) \times \int_{\ln G_0}^{\ln G} \frac{du}{1 + \left(\frac{1}{\psi(r)[1-G_2]-1} \right) e^{-u}} \tag{27}$$

The integration of (26) and (27) is simply done

$$G(r) = \frac{G_0}{G_0 + (1-G_0) \exp \left[-[1 + G_1 \psi(r)] \frac{J_{in}(r)}{J_s} \right]} \tag{28}$$

$$J_{out}(r) = J_s \left[\frac{\psi(r) G_2}{1 - \psi(r)[1-G_2]} \right] \ln \left(\frac{1 + G_0[\psi(r)(1-G_2)-1]}{1 + G(r)[\psi(r)(1-G_2)-1]} \right) \tag{29}$$

Combining (28) and (29) and removing $G(r)$, the relationship between the input-energy and output-energy fluences can be obtained for a double-pass amplifier

$$\exp \left[-\left(\frac{1 - (1-G_2)\psi}{G_2 \psi} \right) \left(\frac{J_{out}(r)}{J_s} \right) \right]$$
$$= \frac{G_0(1-G_2)\psi + (1-G_0) \exp \left[-(1+G_1\psi) \left(\frac{J_{in}(r)}{J_s} \right) \right]}{\{1 + G_0[(1-G_2)\psi - 1]\} \left\{ G_0 + (1-G_0) \exp \left[-(1+G_1\psi) \left(\frac{J_{in}(r)}{J_s} \right) \right] \right\}} \tag{30}$$

Eqs. (30), (23), (24), and (25) show the double-pass amplifier's behavior in the framework of single-pass amplifier model and according to the radial situation, which is called the generalized analytical model of double-pass amplifiers.

Now, we investigate (30) in special states. If the input-energy fluence is much lower than the saturation-energy flux ($J_{in} \ll J_s$), the approximation $G_1 \approx G_2 \approx G_0$ is very appropriate and will be substituted for (23) and (24). In this instance, (30) is simplified further as

$$\exp\left[-\left(\frac{1-(1-G_0)\psi}{G_0\psi}\right)\left(\frac{J_{out}(r)}{J_s}\right)\right]=\frac{\psi G_0+\exp\left[-(1+G_0\psi)\left(\frac{J_{in}(r)}{J_s}\right)\right]}{(1+\psi G_0)\left\{G_0+(1-G_0)\exp\left[-(1+G_0\psi)\left(\frac{J_{in}(r)}{J_s}\right)\right]\right\}}$$
(31)

In the saturation state: $J_{in}\geq J_s$, $G_1\ll G_0$, $G_2\ll G_0$, and $G_1\approx G_2\approx1$; accordingly, (30) is reduced to

$$\exp\left[-\left(\frac{1}{\psi}\right)\left(\frac{J_{out}(r)}{J_s}\right)\right]=\frac{\exp\left[-(1+\psi)\left(\frac{J_{in}(r)}{J_s}\right)\right]}{G_0+(1-G_0)\exp\left[-(1+\psi)\left(\frac{J_{in}(r)}{J_s}\right)\right]}$$
(32)

4 Beam-transfer function

The uniform intensity distribution and Gaussian intensity distribution are the most important items we usually deal with in practice. Hence, we study the function ψ in the following two states.

4.1 Input beam with uniform intensity distribution

For the uniform intensity distribution, the photon density at $z=0$ is given by

$$\Phi_1(r,0,t)=\left|\begin{array}{l}\Phi_0 f(t);\,|r-r_1|\leq a_1\\0\quad;\,|r-r_1|>a_1\end{array}\right.$$
(33)

where $f(t)$ represents the temporal changes in input intensity, Φ_0 is constant, and $2a_1$ is the input beam diameter. By assuming that the pulse's temporal behavior does not change after passing the amplifier, there is a similar expression for the second-pass input beam

$$\Phi_2(r,L,t)=\left|\begin{array}{l}\Phi_0 TG(r,t)f(t);|r-r_2|\leq a_2\\0\qquad;|r-r_2|>a_2\end{array}\right.$$
(34)

Considering (8), (33), and (34), the beam-transfer function is obtained as

$$\psi(r,T)=\left|\begin{array}{l}T\,;|r-r_2|\leq a_2\\0\,;|r-r_2|>a_2\end{array}\right.$$
(35)

4.2 Input beam with Gaussian intensity distribution

For the Gaussian intensity distribution with the spot size of w_1, the input-photon density is given by

$$\Phi_1(r,0,t) = \Phi_0 f(t) \exp\left[-2\left(\frac{r-r_1}{w_1}\right)^2\right] \tag{36}$$

Also, the second-pass input-photon density is defined as

$$\Phi_2(r,L,t) = \Phi_0 f(t) G(r) T \exp\left[-2\left(\frac{r-r_2}{w_2}\right)^2\right] \tag{37}$$

Accordingly, the function ψ is achieved by considering (8), (36), and (37)

$$\psi(r,T) = T \exp\left[2\left(\frac{r-r_1}{w_1}\right)^2\right] \exp\left[-2\left(\frac{r-r_2}{w_2}\right)^2\right] \tag{38}$$

5 Investigation of double-pass amplifier's behavior using the generalized model

Based on (30), Figs. 1 and 2 show the behavior of $G(r)$ and $J_{out}(r)$ for a Gaussian input beam in three states: too far away from saturation ($J_{ino}/J_s = 0.1$), saturation ($J_{ino}/J_s = 1$), and complete saturation ($J_{ino}/J_s = 2.81$), similarly to what we faced in practice. In these calculations, according to the empirical values, we selected $G_0 = 8.804$ for 98 J pumping energy delivered to the lamp, $T = 0.23$, the first-pass input-spot size is 0.88 mm, and the second-pass input-spot size is 0.5 mm. The first-pass input-beam direction is along the amplifying probe's symmetry axis ($r_1 = D/2$) and we selected the second-pass beam's normalized radial position to the amplifying probe diameter (r_2/D) at five different positions from 0.1 to 0.5. As the passing beams' propagation directions approach each other, the beam-interaction effect on the active medium's gain becomes clearer, the output-energy gain and fluence reaches their minimum for $r_2 = r_1$, and $G \approx 1$ for $J_{ino}/J_s \geq 1$.
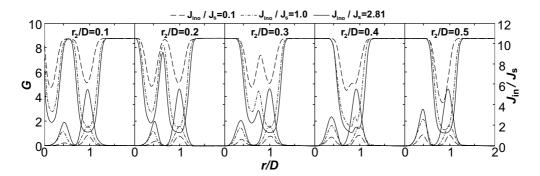

Figure 1: The gain's radial behavior. D is the amplifying probe diameter. $G_0 = 8.804$ for pumping energy 98 J, which is consistent with empirical observations.
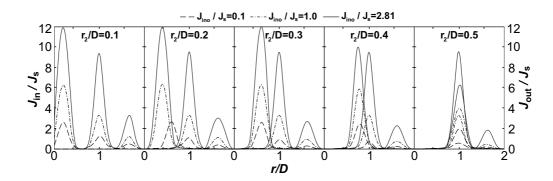
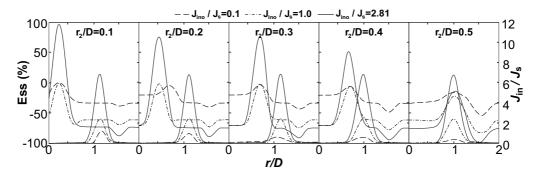Figure 2: The normalized output fluence's radial behavior J_{out}/J_s. $G_0 = 8.804$ for pumping energy 98 J.

Figure 3: The approximate-model error's radial behavior E_{ss} for $J_{in} \ll J_s$.

When $|r_2 - r_1| \leq (w_1 + w_2)/2$ and the beams' directions do not coincide, non-uniform spatial changes in the gain distort the spatial distribution of intensity for the second-pass beam. This impact is evident in Figs. 1 and 2 for $r_2/D = 0.4$.

We define the relative error due to applying (31) and (32) in two special states $J_{in} \ll J_s$ and $J_{in} \gg J_s$ for a Gaussian input beam respectively as

$$E_{ss} = \left[\frac{J_{out-ss}(r) - J_{out}(r)}{J_{out-ss}(r)} \right] \times 100 \tag{39}$$

$$E_{st} = \left[\frac{J_{out-st}(r) - J_{out}(r)}{J_{out-st}(r)} \right] \times 100 \tag{40}$$

Figs. 3 and 4 provide the error-calculation results for five different values of r_2/D. The diagrams indicate that the error due to the simplified model (32) varies between -20 and -50% for the output fluence E_{ss} and $J_{ino}/J_s = 0.1$. As the input fluence rises and exceeds the saturation state, the approximation (31) becomes invalid and an error more than $\pm 50\%$ is observed in the results. Eq. (32) is only valid in the complete saturation state of the active medium's gain. The diagrams of Fig. 4 demonstrate that only when the gain is completely saturated in the first and second passes, (32) leads to acceptable results. This state occurs when the passing beams' directions are very close to each other:
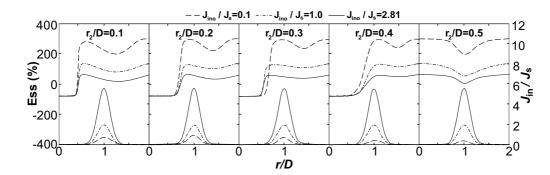
Figure 4: The approximate-model error's radial behavior E_{st} for saturated output fluence.

$|r_2 - r_1| < \max(w_1, w_2)$ and $J_{in} \geq J_s$. This state is observed only in the last diagram of Fig. 4 for $r_2 = r_1$, in which the error is lesser than 40% for $|r - r_1| < w_1$.

When the beams' directions coincide, there is an exact analytical solution (22) to the problem and it can be compared with the results of (30) to study the dependence of the output fluence on input fluence for a double-pass amplifier. Furthermore, for this special state, the results of Frantz–Nodvik model with two separate passes and the gain factor correction [5] can be studied and compared with other methods'. In this calculation the factor of transmission between two passes is equal to one ($T = 1$), and three different values of gain factor ($0.05\,\mathrm{cm}^{-1}$, $0.272\,\mathrm{cm}^{-1}$, and $1\,\mathrm{cm}^{-1}$) have been used to study the results' gain dependence. It can be shown that a small difference about 5% for the average and large values of gain and (J_{in}/J_s) ≤ 1, and this error is negligible for the small values of gain and (J_{in}/J_s) ≥ 1, which suggests that (30) is correct.

6   Comparing analytical results with empirical observations

To confirm the calculated equations in the section 3.2, the output energy of a double-pass Nd:YAG amplifier with effective length of 80 mm was measured according to the distance between passing beams. The single-pass gain G_0 was separately calculated by measuring the input and output fluences and using the Frantz–Nodvik model. The single-pass gain was obtained $0.1589\,\mathrm{cm}^{-1}$, $0.2181\,\mathrm{cm}^{-1}$, and $0.2719\,\mathrm{cm}^{-1}$ for the pumping energy values of 50, 72, and 98 J respectively. In these calculations, the input beam diameter is 3 mm and the amplifying probe diameter is 9 mm.

Employing (23) and (24), for each value of pumping energy, the first-pass and second-pass gains ($G_1(r_1)$ and $G_2(r_2)$) and the output fluence ($J_{out}(r,r_1,r_2)$) were calculated from (30) for a double-pass amplifier. By integrating J_{out} with respect to r, the double-pass amplifier's output energy, $E_{out}(r_1,r_2)$, is obtained according to the center of two passing beams r_1 and r_2

$$E_{out}(r_1,r_2) = 2\pi \int_{r_2}^{D/2} J_{out}(r,r_1,r_2)\, r\, dr \tag{41}$$

Table 1: Properties of Nd:YVO$_4$, Nd:YAG, and Nd:YLF [5, 26, 27].

Properties	Nd:YVO$_4$	Nd:YAG	Nd:YLF
Laser wavelength (nm)	1064	1064	1047(π) 1053(σ)
Peak absorption wavelength (nm)	808	808	792 (π) 797 (σ)
Stimulated emission cross section ($\times 10^{-19}$ cm^2)	25 (π) 7 (σ)	2.8	1.8 (π) 1.2 (σ)
Fluorescence lifetime ($\bar{\ }$s)	90	230	485
Line width (nm)	0.96	0.51	1.47
Peak absorption coefficient (cm^{-1})	31.4 (π) 9.2 (σ)	7	10.8 (π) 3.59(σ)
Absorption bandwidth (nm)	15.7	2.5	4.0 (@792nm) 3.2 (797nm)
Thermal conductivity (W m^{-1}K^{-1})	5	14	6.3
Thermo-optical coefficient ($\times 10^{-6}$K^{-1})	8.5 3.0	7.3	-4.3 (π) -2.0 (σ)
Thermal fracture limit (W cm^{-1}K^{-1})	57.6	94.8	22

Table 2: Small-signal gain and saturation intensity of Nd:YVO$_4$, Nd:YAG, and Nd:YLF.

Type	Small-signal gain	Saturation intensity
Nd:YVO$_4$	25.4	8.30 W mm^{-2}
Nd:YAG	2.52	29.0 W mm^{-2}
Nd:YLF	3.42	21.7 W mm^{-2}

where D represents the amplifying medium diameter.

Eq. (30) is studied with the calculation of output energy according to the distance between the passing beams' centers for $J_{in} \ll J_s$ and $J_{in} \geq J_s$ (Eqs. (31) and (32) respectively for 72 J and 98 J). It is observed that when the distance between beams' directions is more than half the beams' total spot size, the analytical results are completely consistent with the empirical results. In all the states, the input-beam energy is 19.5 mJ and the beam diameter is 2.5 mm. As the beams' directions approach each other, the model largely follows observed empirical behavior and gives smaller values of output energy at 10-20% for propagating two beams along one direction.

Table 1 provides a comparison between the thermal and optical properties of Nd:YV O$_4$, Nd:YAG, and Nd:YLF. Table 2 makes a comparison between the small-signal gain and saturation intensity of them.

The beam profile in the focal region of a beam from a typical multimode fiber looks similar to the solid line in Fig. 5. Fig. 6 makes a comparison between ln($G_{0,G}$) and
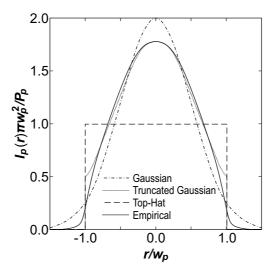
Figure 5: Multimode fiber-coupled pump beams for Gaussian and Top-Hat approximations compared to the empirical results.
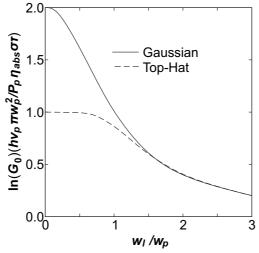

Figure 6: Signal-pump overlap dependence of small-signal gain.

$\ln(G_{0,T})$ versus signal-pump overlap ratio w_l/w_p. Fig. 7 in fact provides gain variation versus input-signal power.

7 Conclusions

The model we devised here is an extension of Frantz–Nodvik model for double-pass optical amplifiers, which can be used to design optical-joint systems with double- and multi-pass amplifiers and to optimize their efficiency.
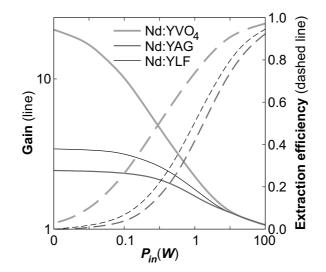
Figure 7: Variation in extraction efficiency and gain vs. input-signal power.

Without need for the numerical solution to partial rate equations of mass contrast and photon density, this model can be used to optimize double-pass amplifiers and multipass amplifiers (whose gain is completely dependent on the distance between beams) through iterating. Despite the assumptions that the optical pulse's temporal behavior does not change after it passes the amplifier, the passing time is much shorter than the input-pulse temporal width, and the transverse distribution of the first-pass beam's intensity is not distorted in spite of beam-interaction effects on optical gain, this model leads to appropriate and acceptable results. The calculation results indicate that the output energy and efficiency of a double-pass amplifier reach their minimum when the two passing beams' directions coincide. As beams move away each other, the interaction between beams declines. In practice, the maximum efficiency is obtained when the distance between beams' centers exceeds the sum of passing beams' spot size. These considerations along with empirical observations and the comparison of results confirm this model's effectiveness.

References

[1] B. M. Wonterghem, J. R. Murray, J. H. Campbell, *et al.* Appl. Opt. 36 (1997) 4932.
[2] W. H. Lowdermilk and J. E. Murray, J. Appl. Phys. 51 (5) (1980) 2436.
[3] J. E. Murray and W. H. Lowdermilk, J. Appl. Phys. 51 (7) (1980) 3548.

[4]   L. M. Frantz and J. S. Nodvik, J. Appl. Phys. 34 (8) (1963) 2346.
[5]   W. Koechner, Solid State Laser Engineering, 5th ed. (Springer, Berlin, 1999).
[6]   M. S. Andrew, G. Cook, and A. P. G. Davies, Appl. Opt. 40 (2001) 2461.
[7]   R. S. Hargrove, R. Grove, and T. Kan, IEEE J. Quant. Electron. 15 (11) (1979) 1228.
[8]   F. Docchi, V. Magni, and R. Ramponi, Rev. Sci. Instrum. 55 (4) (1984) 477.
[9]   H. Okada, H. Yoshida, H. Fujita, and M. Nakatsuka, Opt. Commun. 260 (1) (2005) 277.
[10] M. Pokrass, Z. Burshtein, R. Gvishi, and M. Nathan, Opt. Mat. Exp. 2 (6) (2012) 825.
[11] B. Ren, P. Frihauf, R. J. Rafac, and M. Krstic, Cont. Eng. Pract. 20 (7) (2012) 674.
[12] M. Petrarca, M. Martyanov, M. C. Divall, and G. Luchinin, Quant. Elect. 43 (3) (2011) 306.
[13] A. C. Erlandson, S. M. Aceves, A. J. Bayramian, et al. Opt. Info. Base. 1 (7) (2011) 1341.
[14] S. C. Pearce, L. M. Ireland, and P. E. Dyer, Opt. Commun. 255 (2005) 297.
[15] R. B. Kay, D. Poulios, D. B. Coyle, P. R. Stysley, and G. B. Clarke, Quant. Elect. 47 (5) (2011) 745.
[16] W. R. Donaldson, D. N. Maywar, J. H. Kelly, and R. E. Bahr, Opt. Info. Base. 28 (3) (2011) 445.
[17] X. Ma, J. Bi, X. Hou, and W. Chen, Optics & Laser Tech. 43 (3) (2011) 559.
[18] R. Geng and S. Jian, Optik-Int. J. Light Electron. Opt. 122 (9) (2011) 804.
[19] G. Wagner, V. Wulfmeyer, and A. Behrendt, Appl. Opt. 50 (31) (2011) 5921.
[20] L. D. Mikheev, V. I. Tcheremiskine, O. P. Uteza, and M. L. Sentis, Prog. Quant. Elect. 36 (1) (2012) 98.
[21] N. N. Ilichev, A. V. Larikov, and A. A. Malyutin, Sov. J. Quantum. Electron. 20 (11) (1991) 1336.
[22] Z. Yang, J. Zhang, and Y. Zhang, J. At. Mol. Sci. 2 (2) (2011) 143.
[23] S. Y. Zhang, J. At. Mol. Sci. 1 (4) (2010) 308.
[24] A. Heidari and M. Ghorbani, J. Mod. Phys. 3 (3) (2012) 278.
[25] A. Heidari, M. Zeinalkhani, A. Nabatchian, *et al.* Mod. Appl. Sci. 6 (5) (2012) 82.
[26] O. Svelto, Principles of Lasers, 4th ed. (Kluwar Academic Publishers, New York, 1998).
[27] Z. Xiong, Z. G. Li, W. L. Huang, and G. C. Lim, IEEE J. Quant. Electron. 39 (8) (2003) 979.

Appendix

As a result of long extending tails at the first or too short tails in the latter, resolving absorption spectra in the wavenumber scale into the exact Lorentzian or into the exact Gaussian peaks are inadequate. Also, such peaks that appear asymmetric have their shorter tails on the low-wavenumber side. Therefore, a Lorentzian function is modified to show an exponential decay on its short wavenumber side through

$$B(\widetilde{\nu}) \equiv I_0 \frac{(\Gamma/2\pi)}{(\widetilde{\nu} - \widetilde{\nu}_0)^2 + (\Gamma/2)^2} \cdot \frac{1}{1 + \exp\left[\frac{(\widetilde{\nu} - \widetilde{\nu}_0) - \Gamma/2}{\Gamma/2}\right]} \tag{42}$$

This "one-side truncated" function shows a single peak, whose position is given by $\widetilde{\nu}_p = \widetilde{\nu}_0 + 0.07\Gamma$, the half-maximum full width is defined as $\Delta\widetilde{\nu}_{FWMH} = 0.9625\Gamma$, and the integrated intensity is $I \equiv \int_0^\infty B(\widetilde{\nu})\, d\widetilde{\nu} = 0.60544 I_0$. Note that the band integrated intensity correlates with its transition oscillator strength through

$$f = \frac{3mc^2}{\pi n e^2} \frac{I}{N} \tag{43}$$

where m represents electronic mass, e electronic charge, c speed-of-light constant, n medium refractive index, and N denotes ion concentration.